Scientia Iranica B (2014) 21(2), 414–424

SCIENTIA IRANICA

Sharif University of Technology
Scientia Iranica
Transactions B: Mechanical Engineering
www.scientiairanica.com

A new experimental approach to investigate the induced force and velocity fields on a particulate manipulation mechanism

M. Zabetian, M.B. Shafii*, M.H. Saidi, M.S. Saidi and R. Rohani

Center of Excellence in Energy Conversion (CEEC), School of Mechanical Engineering, Sharif University of Technology, Tehran, Iran.

Received 26 October 2012; received in revised form 8 September 2013; accepted 10 December 2013

KEYWORDS
Particle manipulation;
Induced force;
Induced motion;
Minichannel;
Microscopy;
Image analysis.

Abstract. Identification and minimization of error sources are important issues in experimental investigations. Mainly in micro-scale problems, precise settings should be applied to high-tech test beds to reduce disturbance and induced motion. An experimental study is conducted to assess the role of induced forces and velocity fields in a particulate system used for particle identification and separation. Two main effects caused by disturbances are sampling errors and induced motion in the channel, either on fluid or dispersed phases. Different disturbance scenarios are implemented on the test bed and then the system response is reported. In order to assess induced motion as a result of applied forces, microscopic imaging of particle movement in the channel and image processing of the results, are performed. Results of particle sampling indicate that optimized pneumatic settings should be implemented to secure a safe level of sampling error. Results for induced flow show that the velocity field can affect the operation of the manipulation mechanism. Methods for capturing the induced force and velocity fields can be implemented in the relevant applications, such as micro-particle systems and cellular studies.

1. Introduction

Experimental study of micro-scale problems is usually associated with high precision and accuracy. An important issue in micro-fluidic investigation is identification and minimization of disturbances. Disturbances can affect the main physics to be investigated and may mislead the results. Specifically, when dealing with micro and nano-flow containing particles, disturbances are capable of applying forces and the resultant motion of the fluid or dispersed phase. The magnitude of the induced velocity field can be comparable to the main flow field. Consequently, it is crucial to identify and compute the induced forces and velocity fields.

Disturbances in micro-flow can be generated by surrounding media or test rig components. Air-borne noises can induce forces in different elements. For instance, rotary elements such as cooling fans and ventilation systems can apply forces to air-fluid interfaces and channel walls [1,2]. Other rotary or frequency generating devices can apply forces to flow boundaries as well. For instance, lasers and ultrasonic baths are devices that can generate motion in fluid due to the mentioned effect. In this regard, we focus on these two sources of disturbance on a particle manipulate ion mechanism. Here, some relevant work is reviewed.

Regarding the induced fields, it is important to identify the forces applied to a particulate material. Particles can be manipulated either passively or ac-

*. *Corresponding author. Tel.: +98 21 66165675;
Fax: +98 21 66000021
E-mail address: Behshad@sharif.edu (M.B. Shafii)*

tively. Passive forces, such as Van der Waals, Brownian, and wall induced forces, are not capable of high levels of controllability, consistency and repeatability [3].

Yang et al. [4] reported noise measurement in particle size analysis using a dynamic light scattering technique. They mentioned two sources of noise: sample preparation and laser light fluctuations. Sampling error can cause false data in size measurement experiments. Nitschke and Schmidt [5] presented a model to describe the re-entrainment of settled particles into the flow using film theory for fluids. For this purpose, they implemented adhesive and removal forces in their model. Similarly, some other models are presented to analyze wall-particle interaction using microscopic imaging [6-8].

Numerous studies have explored vibration induced motion on fluid [9-11] and excitation of the wall to produce fluid flow [12-14]. Akiyama et al. [15] presented induced convection applied by the vibration of a vessel wall. Particles in the forms of granular beads with a size range of 1-100 μm were used in experiments. Despite comprehensive case studies, only qualitative path lines of particles were presented. Jang et al. [16] used piezoelectric elements coupled with thin diaphragms to induce motion in a fluid. Bulk fluid motion and flow hydrodynamics have been studied experimentally via the PIV method with 2 μm spatial resolution.

Image analysis techniques have been widely used to characterize particulates [17-19] and calculate particle trajectories [20]. Kashdan et al. [21] conducted some experiments to assess the accuracy of their digital image processing technique for sizing fuel droplets ranging from 5 to 30 μm. Results obtained were compared with a technique called Doppler anemometry. They concluded that the image analysis technique can be developed into one micron size while keeping its accuracy. Wesely et al. [22] used dynamic image analysis for particle identification and measurement of particle size and concentration to study the overlapping of clusters of particles.

Wedd [23] reported a simulation study to predict the accurate size and quantity of a mixture of monodispersed particles used for calibration purposes. The study emphasized that for the method to succeed, there should be accurate weighing and particle handling techniques associated with sizing accuracy. Experimental studies also used reference mono-dispersed particles for validation of the proposed techniques [6,24,25]. Accurate image analysis techniques also are used in particle sizing applications [26-29].

Capturing the movement of micro and nanoparticles is investigated by various studies, both theoretically and experimentally [30-32]. Studies are mainly focused on imaging techniques including Particle Tracking Velocimetry (PTV), Particle Image Velocimetry (PIV) and microscopic image analysis schemes [32]. Among mentioned techniques, particle tracking via image analysis is considered more especially for dilute suspensions [33-35].

Hao et al. [36] used micro-Particle Image Velocimetry (PIV) to measure slip velocity on the wall of approximately 8% of the centerline velocity. Patrick et al. [37] reported near-wall Red Blood Cell (RBC) motion of high-hematocrit blood in a rectangular microchannel using a combination of fluorescent dye labeling, time-resolved scanning confocal microscopy, and micro-particle image velocimetry.

Despite comprehensive work published on the subject of force and velocity measurements in minichannels, no work has been reported regarding direct measurements of force and velocity fields induced by different disturbances. The magnitude of the induced fields can mislead the reported results in laboratory experiments dealing with particulate flow, covering lab on a chip devices and drug production processes. Moreover, different types of disturbance have not been categorized and assessed in detail. Devices such as laser, which is widely used to obtain velocity and temperature fields in microfluid applications, can induce force and motion on fluid and particles as well. Considering the fact that fluid viscous damping can change the magnitude and spectrum of induced forces applied to particles suspended in liquid, conventional vibration measurement techniques are unable to calculate the force and velocity fields applied to the particulate flows.

This investigation is aimed at presenting a new method to measure force and velocity fields applied to a typical particulate flow system subjected to different disturbances. Direct measurement of the induced weight and particle motions makes it possible to assess the role of the disturbances on the physics being studied. Compared to similar investigations, this work proposes an experimental tool to calculate the effect of each disturbance source on the induced force and velocity fields. Different sources have been discussed, including: airborne, ground, impact, walking and laser induced disturbances. The proposed assessment techniques can be implemented on similar laboratory environments concerning particulate flows.

2. Materials and methods

In this study, an anti-vibration table equipped with air springs is used to assess the level of induced fields generated by surrounding and rotary devices in a minichannel. Discussion about vibration spectrum is not in the scope of this work and the goal is to find out the magnitude of force and velocity fields at the location of the test bed components.

As a first step, the disturbance sources in the

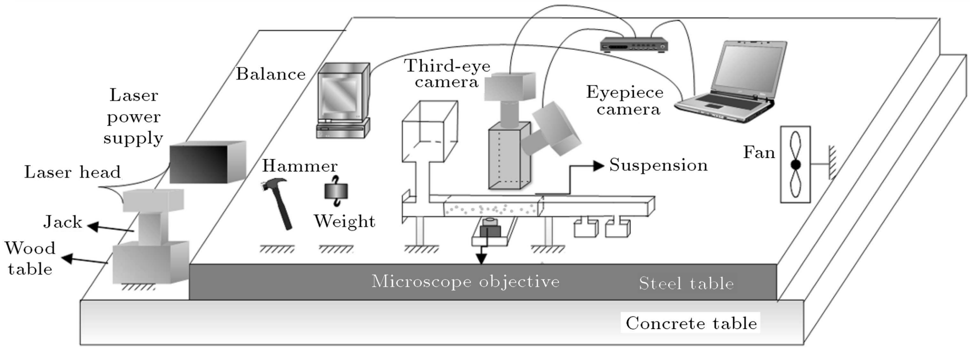

Figure 1. Schematic view of the experimental set up including particulate manipulation mechanism and measurement devices.

laboratory environment have been categorized. The main sources are airborne (from fans or ventilation systems), ground, impact and walking. In order to assess induced forces, mass sampling measurements are performed for initial pneumatic and optimized pneumatic settings (the settings at which the induced forces are minimized) to obtain conditions resulting in minimum induced fields. In addition, a set of tests is designed to determine the induced flow and particle motion in the channel produced by the above-mentioned sources.

2.1. Design of experiments

In this section, we report the design of experiments in order to estimate the magnitude of the induced velocities caused by external disturbances. The design of the experiments can be extended to similar applications in microfluidics and particulate flow. In addition, the disturbance quantity is measured and represented by the induced force using a new method, which describes the behavior of the applied disturbances. Figure 1 shows the schematic view of the test bed and devices used for studying the induced fields. As can be seen, the manipulation mechanism, including the laser source and suspension passages, is installed on the steel anti-vibration table. The steel table is installed on a concrete anti-vibration table in order to minimize the magnitude of vibration on the position of test bed components. A schematic view of the measurement points is depicted in Figure 2. Points 1-4 are located on the ground with no vibration isolators, whereas points 5-8 and 9-13 are on the concrete and steel anti-vibration tables, respectively; the steel anti-vibration table was unbalanced when the experiments were begun. The results of our tests showed that point no. 9 had the minimum values of induced fields. Therefore, the microscope and other test bed components are installed near point no. 9.

2.2. Testing apparatus

The manipulation mechanism consists of the colloidal suspension of micro-particles dispersed in water (Figure 1). Using dispersion techniques, the sedimentation rate is minimized. The micro-manipulation mechanism is designed and fabricated to detect and separate colloidal suspensions in the size range of 10 to 100 microns.

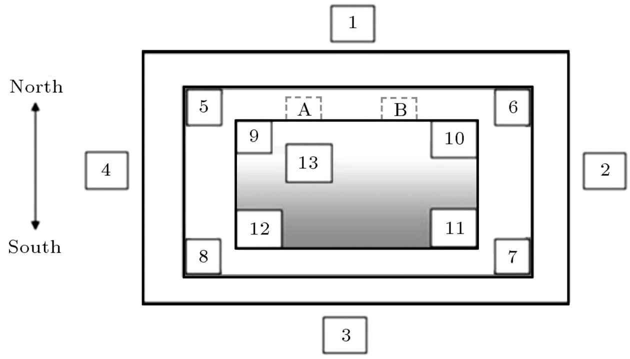

Figure 2. Schematic view of anti-vibration tables and measurement points.

As mentioned before, the sources of disturbance can apply forces and motion on the set up components, particularly on the suspended particles to be manipulated. Two major instruments used in the mechanism are the microscopic balance and the optical microscope, which we have used to capture both forces and motions. As such, this gives us a more realistic judgment about the magnitude of error induced by surroundings and the role of scenarios applied to minimize them.

Microscopic balance is equipped with a recording system (with frequency of 5 Hz) that enables us to record the induced forces in terms of weight with a precision of 10 micro-grams. The balance is placed near the main manipulation mechanism to record the magnitude of induced force near the minichannel.

The manipulation mechanism uses a conventional light microscope equipped with two imaging systems. Table 1 shows the main features of the imaging systems. The first system is a high-resolution (10 megapixels in the video mode) CCD camera mounted on the third eye of the microscope. The small pixel size of the camera enhances its capability to identify objects as small as 0.11 μm (Table 1). The second imaging system

Table 1. Imaging system general features.

Imaging type	Exposure time range	Maximum field of view (mm^2)	Best spatial resolution (μm)	Fps range
Third-eye CCD camera	1-65000 μs	3.189	0.113	1-21
Eye-pieces CMOS camera	1-200 ms	8.842	0.51	1-25

is to capture relatively wide field of view images, up to 8.8 mm^2 (Table 1). This helps to have an overview of particle movement in the channel. A simpler video camera mounted on the eyepieces of the microscope is used for this purpose. Total magnification of 80× can be achieved using these imaging mechanisms. The above-mentioned imaging systems are used to measure colloidal suspension transport through the minichannel. By choosing the appropriate frame rate and magnification, the flow field can be captured with maximum spatial resolution and the desired field of view (Table 1).

The first step in the digital image processing of acquired images is calibration of video pictures against a distance standard (i.e. a ruled glass micrometer). Video tracking of moving particles using a cross correlation technique is implemented. Considering a single image of particles, particle detection and size distribution can be derived from image processing. Comparing two consecutive images, the corresponding displacement vector of each particle is calculated with the accuracy of half a pixel. These results are useful in finding the velocity field of particles subjected to external forces.

3. Measurement of the induced fields

Induced forces in terms of weight are measured using the sensitive balance. As mentioned before, different kinds of disturbances can exert force on the particle manipulation mechanism. The force is transmitted on the table top through the damping system. As such, the amplitude and its spectrum are changed. The anti-vibration table can be adjusted to achieve the desired pneumatic settings. Specifically, air springs pressure and auto-level conditions can be set to achieve the suitable damping level. The experiments are designed to estimate the magnitude of the mass error and obtain settings for correct mass sampling of micro-particles. Depending on the direction of the force applied to the balance, the induced mass can be either positive or negative.

Common tools for applying standard disturbances, including hammers, fans and standard weights, are used in the experiments. A laser is one of the main parts of the particle separation mechanism. It can also induce force and motion, due to its cooling fan. Hence, the effect of the isolation of the laser from other parts on the induced force is studied. Air springs are initially charged in the range of 2-3 bars, and weight recording is conducted for the current and desired settings, in response to the applied disturbances. In order to achieve the optimized pneumatic settings, air springs are adjusted with charge in the range of 4-6 bars.

3.1. Induced force for initial settings and optimized settings

Time variation of the induced forces, due to disturbances generated by impact, walking and laser cooling fans, is presented. Results are shown in terms of induced weight versus data number. Data can be saved by maximum frequency of 5 Hz by a capture card to a computer. Therefore, data acquisition of experiments with duration less than 3 minutes is done by a frequency of 5 Hz. In contrast, for disturbance sources with longer effects, a frequency of 1 Hz is used.

All tests, during which the disturbance generation sources exist in a short time, will continue until steady state response approaches zero. The main criteria of the system response include rise time, maximum overshoot, settling time, and steady state error. Rise time, which is a function of disturbance frequency and its response time, depends on the disturbance type. To receive an accurate assessment, the experiments are repeated three times and repeatability is proved.

The walking test is performed for period of 5 seconds on a concrete table and results are depicted in Figure 3. As can be seen in Figure 3(a), the time required for the system steady state response to become zero is about 210 data points (equivalent to 42 seconds). For optimized settings, the settling time is about 65 data points (equivalent to 13 seconds), while there is more fluctuation in weight compared with initial settings.

The next experiment is about applying impact as a disturbance on the steel table. A standard 1 kg weight released from a point located 30 cm above the table implements the impact. Results of the experiments for two settings are shown in Figure 4. Based on the results for initial settings, the disturbance with an overshoot of 1.2 mgr causes an oscillation in the system that is damped after data of 139, or an equivalent duration of 21 seconds (Figure 4(a)). After this time, the steady state response becomes zero. The mean value of induced weight during the experiment is 87 μgr. Figure 4(b) indicates that optimized settings have a faster response when absorbing the disturbance

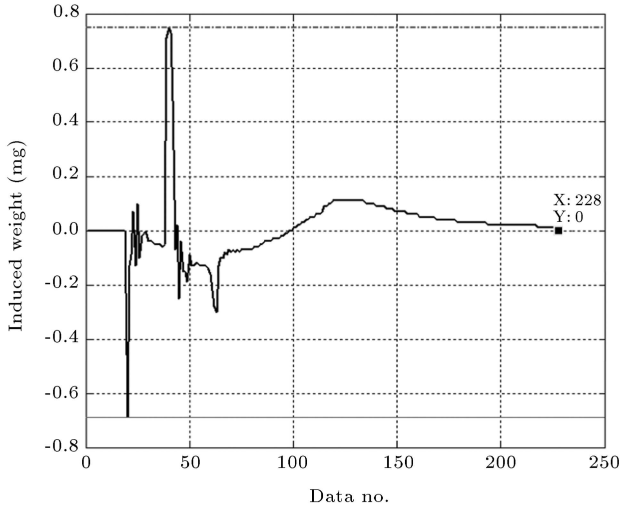

(a)

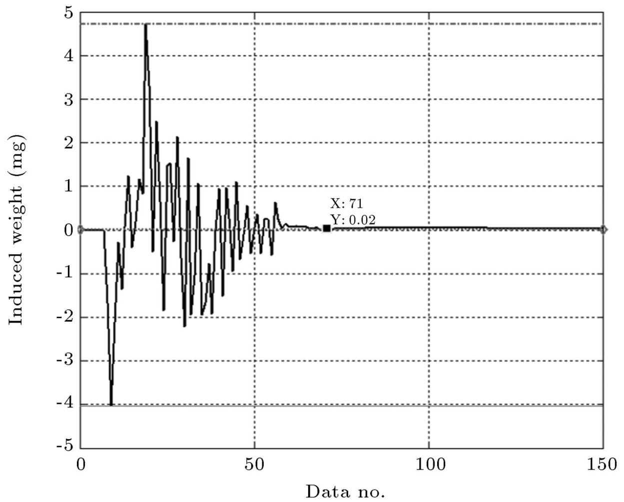

(b)

Figure 3. Comparisons of induced weight in walking test for initial settings (a) and optimized settings (b).

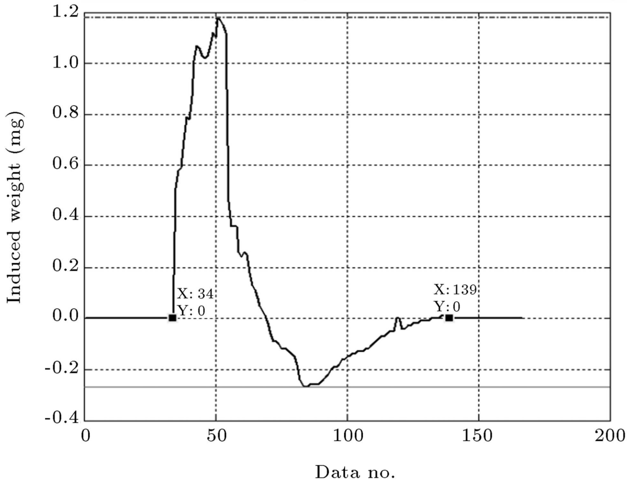

(a)

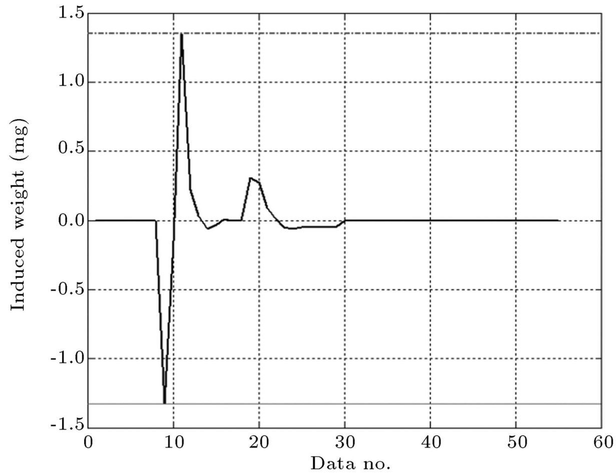

(b)

Figure 4. Induced weight versus data number while applying impact on the table for initial settings (a) and optimized settings (b).

Table 2. Statistical information of impact on the table for initial and optimized settings.

Statistical parameter	M_i (mgr)	M_{Opt} (mgr)
Maximum	1.18	1.35
Minimum	-0.27	-1.33
Mean	0.0869	0.0065
Standard deviation	0.345	0.273

compared with the initial settings. In both cases, the induced weight is zero after the settling time.

More detailed comparison of the two settings is presented in Table 2. The range of induced weight for optimized settings is larger than the initial settings for both walking and impact experiments, but the mean and standard deviation is less than initial settings. This implies that the optimized setting is exposed to more induced forces, due to the higher air charge in the springs, but has a faster and stronger performance in absorbing applied disturbances.

3.2. Induced force by laser cooling fan

Among the manipulation mechanism components, the laser cooling fan is considered critical, and one which can have more effect on the system. This hypothesis is proved by recording the temporal variations of the induced force when the laser is set up on the steel table near to the minichannel. Therefore, in the next test, the laser fan induced force is studied. As can be seen from Figure 1, the scenario is designed to minimize the induced force of the laser fan by isolating the laser from the main mechanism components, such as the minichannel and microscope. For this purpose, the laser is placed on the wooden table, which is installed on the concrete table. For further reduction in the induced force, the laser is placed on a laboratory jack

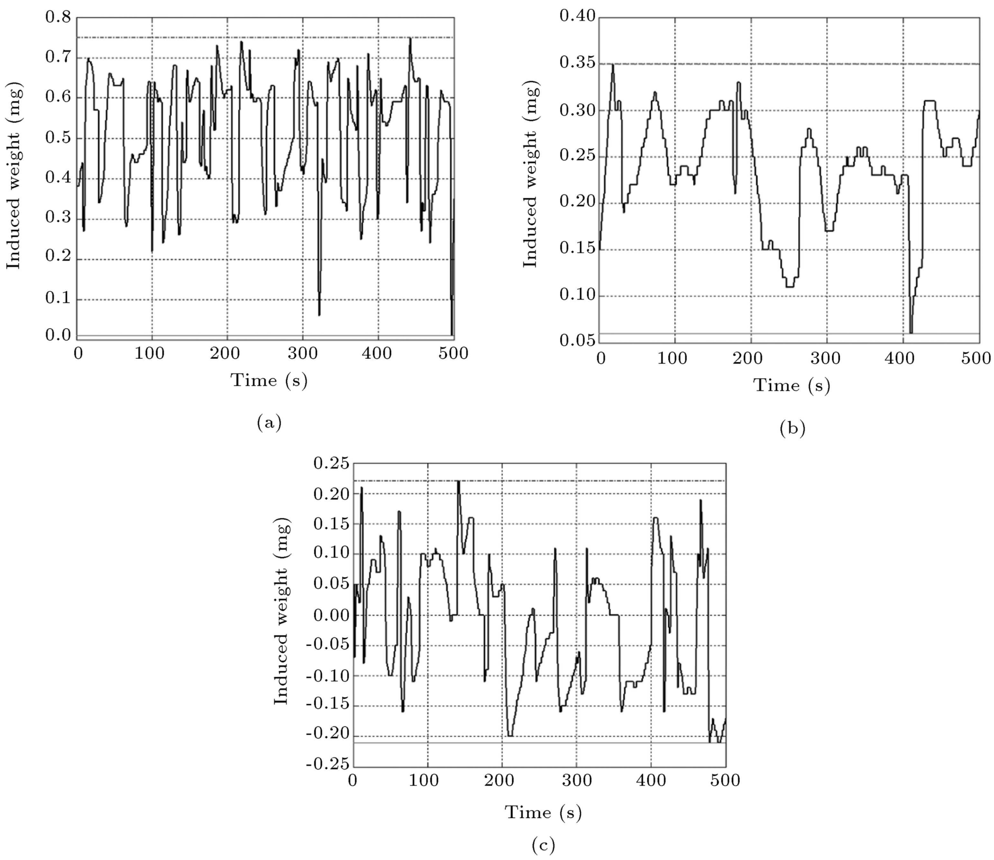

Figure 5. Comparison of induced weight profiles for laser operating on the steel table at optimum pneumatic settings and for three different positions: (a) laser on the steel table near other parts; (b) laser isolated from mechanism and on the concrete table; and (c) laser isolated from mechanism and on the jack.

and the results for induced force are compared with previous cases. Figure 5 shows the results for three mentioned cases. The first case is the laser operation on the steel table. The induced force profile for this case (Figure 5(a)) indicates that there is a strong induced field with a fluctuating nature on the balance. Due to the fact that the laser cannot be turned off during the particle manipulation experiments, it is crucial to reduce the induced force. Figure 5(b) shows the temporal variation of the force profile for the second case, in which the laser is isolated and is operating on the small table installed on the concrete table. As can be seen, there is a noticeable decrease in the magnitude of the induced force during the period of experiment. Finally, operating the laser on the jack, according to Figure 1, leads to the best reduction in the magnitude of induced force. Table 3 describes the comparison of the three cases in detail. By surveying the results, it can be seen that the mean value of the force is reduced from 482 μg in case 1 to 17 μg in case 3. The mean value in case three is comparable to the balance accuracy of 10 μg. This implies that the laser fan effect is minimized to a safe level by the applied scenario. Therefore, in the next experiments, the laser was isolated from the minichannel, in accordance with case 3.

Table 3. Comparison of induced weight data for laser operating on the steel table (Case 1) isolated on the concrete table (Case 2) and isolated on the laboratory Jack (Case 3) at optimized settings.

Statistical parameter	M_1 (mgr)	M_2 (mgr)	M_3 (mgr)
Maximum	0.98	0. 35	0.22
Minimum	0.01	0.06	-0.21
Mean	0.4826	0. 2368	-0.0173

3.3. Induced motion of microscopic particles suspended in the liquid exposed to disturbances

After analyzing the induced forces due to the lack of air charging and the laser cooling fan effect, the set up was reconfigured with optimum charging and laser position. The other part of the experiments was devoted to the measurement of induced velocities caused by the major disturbance sources under optimized conditions. According to the test procedure described in section 2.1, dynamic image analysis is used to characterize the induced motion of microscopic particles due to disturbance sources. As mentioned before, two imaging systems are used to study the particle movements, in

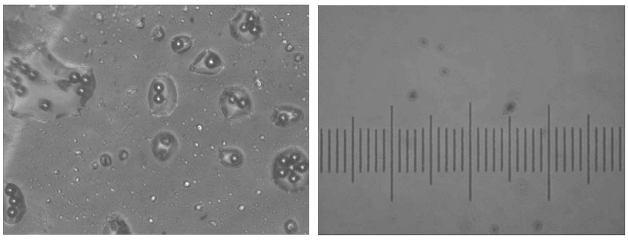

(a) (b)

Figure 6. Image calibration for (a) mono-dispersed particles, (b) poly-dispersed particles and 20× magnification.

order to have an overview of the flow field, besides keeping the desired accuracy in particle tracking.

The first step in image analysis is calibration of the captured images. Figure 6(a) shows a still image of 15 μm mono-dispersed particles settled on the minichannel wall. Image calibration is performed using a micrometric scale bar (Figure 6(b)).

3.4. Induced flow by airborne disturbance

As a next step, the induced motion of mono-dispersed particles in the minichannel is studied. Micro-particles are suspended homogeneously in water and the effects of fan induced motion, random noise and impact on the table are investigated. Figure 6 shows microscopic images of particle movements in the minichannel as a result of airborne disturbance. The fan motor is shut down at $t = 0$, so there is no source of disturbance in the period of the experiment. As such, we expect a decaying behavior in the particle movements. Experiments have been repeated in order to prove the repeatability of trends and the accuracy of the results. Figure 7(a) and (b) shows the relatively fast movement of 15 μm particles in an axial direction. Thirty seconds after turning the fan off ($t = 30$ s), the magnitude of particle displacements, labeled C, D and E, is much smaller than particles A,B and C at $t = 10$ s (Figure 7(c) and (d)).

In order to assess the role of airborne disturbance in the minichannel, a comparison study for fan experiments is conducted. Results are illustrated in Figure 8(a) and (b). When the fan is not running (Figure 8(a)), there is still an airborne effect and background noise with a mean velocity of 6.9 μm/s. As can be deduced from Figure 8(b), airborne effects can generate a strong velocity field compared with the velocity scales of particles in the manipulation mechanism. Due to the fact that the channel is in contact with air on both sides, the temporal velocity profile has a fluctuating nature.

3.5. Induced flow by Impact test

Mono-dispersed particles have been used as the media for the impact tests. A typical result for the impact experiment is demonstrated in Figure 9. As mentioned before, at an optimum pneumatic setting, an induced velocity field with a magnitude of 10-15 μm/s exists because of particle sedimentation and external sources of disturbance.

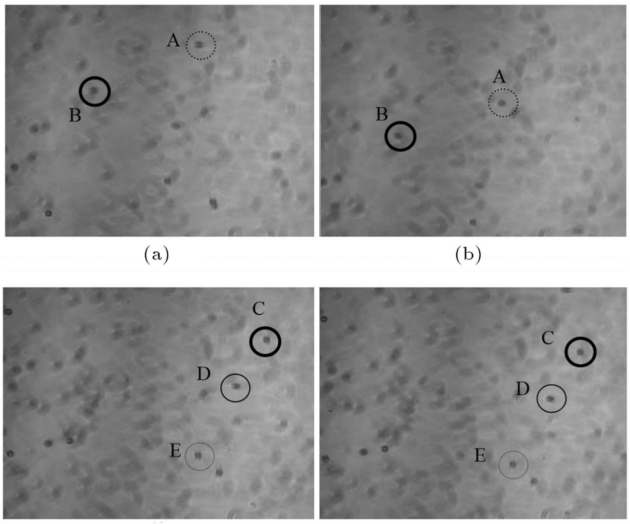

(a) (b)

(c) (d)

Figure 7. Microscopic images of migration of micro-particles in water due to the airborne disturbance: (a) Position of particles A and B at $t = 9$ s; (b) position of particles A and B at t=10 s; (c) position of particles C, D and E at $t = 29$ s; and (d) position of particles C, D and E at $t = 30$ s.

This offset exists for any experiment. In the case of Figure 9, an initial velocity of 10.5 μm/s is recorded, while subject to the impact test at t =2 sec. As can be seen, a sudden rise in particles velocity is captured with a peak value of 165 μm/s. Similar to the other experiments, the damping mechanism of the system is responsible for the decaying of the fluctuating nature of the velocity field. Results show that after 30 seconds, the steady state response is nearly achieved, with a final speed of 15 μm/s.

3.6. Comparison of the induced fields

To summarize this part of the study, we compare the results of the induced velocity fields due to the applied disturbances. Expressed results in Table 4 indicate that the fan induced disturbance has maximum impact on suspension with the maximum amplitude of 897 μm/s. This indicates that the source of disturbance (e.g. ventilation fan) must be turned off during the experiments.

Detailed error analysis is performed to calculate the maximum error caused by the measurement apparatus. For mass sampling, the sensitive balance has an accuracy of 10 μg. For optimized pneumatic settings, the critical induced weight is generated by the laser with a mean value of 17 μg (Table 3). For particle velocity measurement using image processing, a maximum relative error of 2.8% is calculated for conditions of minimum particle displacement in the channel.

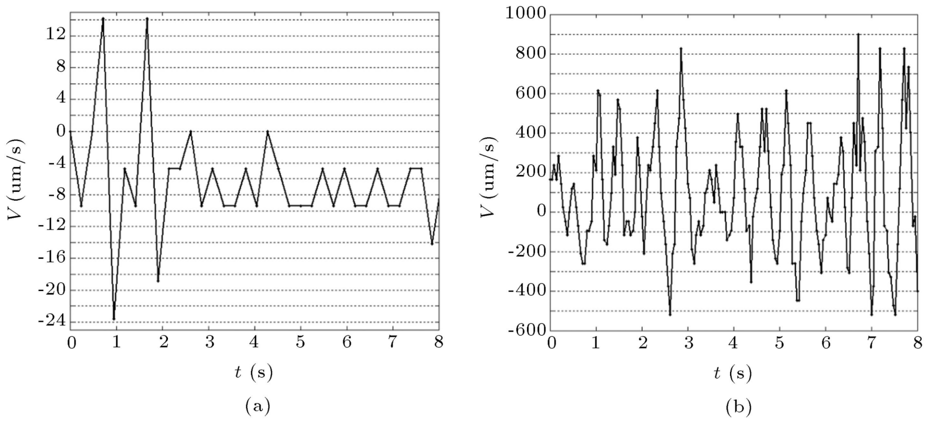

Figure 8. Time variation of induced velocity field in the minichannel due to airborne disturbance: (a) While fan is off; and (b) while fan is turned on.

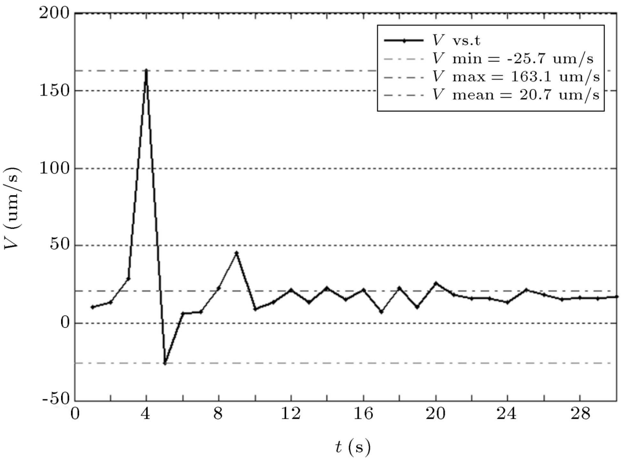

Figure 9. Variations of average induced velocity of mono-dispersed particles in the minichannel subject to the impact test at $t = 2$ s on the steel table.

Table 4. Comparison of maximum induced velocities of micro-particles.

Experiment	**Maximum velocity (μm/s)**
Fan	897
Impact-concrete	137
Impact-steel	162
Random disturbance	160

4. Concluding remarks

Induced velocities due to disturbances can affect the results of velocity measurements in microfluidic and particulate flows. In this paper, we described the precise measurements of induced forces and velocity fields on a test bed and flow passages, using mass recording and microscopy, respectively. The presented methods are capable of measuring the effect of various sources of disturbance applied to typical microfluidic test beds, as well. Main disturbance sources, including airborne, impact, walking and laser fan, are considered in the study, and the experiments have been organized into two sections, including force and velocity measurements.

Results of weight measurement indicate that optimum pneumatic settings (with an air pressure range of 4-6 bars) should be applied to the test bed and mass sampling should be done after the settling time of the existing disturbance.

Tests are designed and done at initial (air springs pressure of 2-3 bars) and optimized (air springs pressure of 2-3 bars) settings. Comparison of the results of two cases shows that the time domain response of the system is improved in charged settings. In addition, the system settling time and steady state error of each setting is analyzed to characterize the test bed. Regarding the induced force by a laser cooling fan and ultrasonic bath, isolating these devices from the main manipulation mechanism is accomplished, and a considerable reduction in magnitude of the induced weight is reported. Presented error analysis shows that maximum error in mass sampling is less than 10% for optimum conditions and the absolute value of induced weight can be reduced to 50 ugr. Therefore, applying the appropriate air charging and isolation of the rotary devices is mandatory in the microfluidics experimental set ups.

By securing the disturbances caused by ground and rotary devices, the level of the induced force can be reduced close to 17 μg, which is acceptable in microfluidic experiments. The other sources, such as impact and airborne disturbances, can generate much more induced forces and velocities. Therefore, to achieve an acceptable level of induced velocities, the remaining experiments have been conducted with secured conditions by optimum charging and isolated laser machines.

Considering induced particle motion in the minichannel, specific experiments have been designed and implemented. The induced flow directly drives particles in an axial direction with small lateral deviations resulting from random fluctuations. While there is homogeneous settling of particles perpendicular to the imaging plane, this leads to relatively small out of focus capturing of particle movements. Results show that air-borne disturbances can induce relatively high magnitude velocities in the channel. Specific consideration should be taken into account, in order to minimize the effects of the induced fields.

Lastly, it is also worth mentioning that the proposed techniques can be considered a tool for direct measurement of the induced effects on the microfluidic related test beds. In comparison with the available methods, such as vibration measurement, the proposed technique gives a truer value of error on the parameter to be studied, such as the motion of micro-particles in liquid. Without implementation of the techniques, the reported results can be affected by error sources and may mislead the drawn judgments.

The presented techniques can also be used to characterize particulate systems and calculation of geometrical and flow characteristics. This investigation can also be developed for use in other applications encompassing molecular and cellular studies, fine positioning and manipulation using electron microscopy techniques (SEM and TEM) and micro-particle manipulators such as optical tweezers. All the mentioned applications deal with relatively high precision measurement techniques and the sources of disturbances should be removed or controlled to secure the level of induced force and velocity fields.

Acknowledgement

This research was funded by the Industrial Development and Renewing Organization (IDRO) as a joint research project with Sharif University of Technology (The contract No is SBDC-03-8880). The authors appreciate their financial support. We are also grateful to Professors B. Rashidian and A. Bakhshi for their valuable scientific and technological support of this work, without which it could not have been concluded.

Nomenclature

D	Diameter (m)
F	Force (N)
g	Gravitational acceleration (ms^{-2})
L	Length (m)
m	Mass (kg)
n	Number density (#/m^3)
t	Time (s)
V	Volume (m^3)
U	Velocity (ms^{-1})
x	Axial coordinate (m)

Subscripts

f	Final
i	Initial
max	Maximum
mean	Average
min	Minimum
P	Particle
s	Suspension
W	Wall

Prefixes

m	Mili
μ	Micro

References

1. Bobrovnitskii, Y.I. and Pavic, G. "Modelling and characterization of airborne noise sources", *Journal of Sound and Vibration*, **261**, pp. 527-555 (2003).
2. Lin, C.N. "Analysis of three-dimensional heat and fluid flow induced by piezoelectric fan", *International Journal of Heat and Mass Transfer*, **55**, pp. 3043-3053 (2012).
3. Kayani, A.A., Khoshmanesh, K., Ward, S.A., Mitchell, A. and Kalantar-Zadeh, K. "Optofluidics incorporating actively controlled micro-and nano-particles", *Biomicrofluidics*, **6**, pp. 031501-031501-32 (2012).
   Kayani, A.A. et al. "Optofluidics incorporating actively controlled micro-and nano-particles", *Biomicrofluidics*, **6**, pp. 031501-031501-32 (2012).
4. Yang, H., Zheng, G. and Li, M. "A discussion of noise in dynamic light scattering for particle sizing", *Particle & Particle Systems Characterization*, **25**, pp. 406-413 (2008).
5. Nitschke, D. and Schmidt, E. "A new approach to model the re-entrainment of settled particles based on film theory of fluid mass transfer processes", *Particle & Particle Systems Characterization*, **26**, pp. 58-68 (2009).
6. Hein, K., Hocke, T., Stintz, M., Ripperger, S. "Analysis of adhesion forces between particles and wall based on the vibration method", *Particle & Particle Systems Characterization*, **19**, pp. 269-276 (2002).
7. Sidorenko, I., Looi, A.Y. and Rhodes, M. "Particle motion near the wall of a fluidized bed at elevated pressure", *Industrial & Engineering Chemistry research*, **43**, pp. 5562-5570 (2004).
8. Sonnenberg, J.P. and Schmidt, E. "Numerical calculation of London-van der Waals adhesion force distributions for different superquadric shaped particles", *Particle & Particle Systems Characterization*, **22**, pp. 45-51 (2005).

9. Chung, S. and Vafai, K. "Vibration induced mixed convection in an open-ended obstructed cavity", *International Journal of Heat and Mass Transfer*, **53**, pp. 2703-2714 (2010).

10. Parsa, A., Srinivasan, S. and Saghir, M.Z. "Impact of density gradients on the fluid flow inside a vibrating cavity subjected to soret effect", *The Canadian Journal of Chemical Engineering*, **91**(3), pp. 550-559 (2012).

11. Sánchez, I., Darias, J. and Michelangelli, O. "Vibration induced granular flow through an elbow", in *International Congress on Agricultural Engineering* (2012).

12. Stan, C.A., Ellerbee, A.K., Guglielmini, L., Stone, H.A. and Whitesides, G.M. "The magnitude of lift forces acting on drops and bubbles in liquids flowing inside microchannels", *Lab on a Chip 13*, pp. 365-376 (2013).

13. Wang, L., Luo, Z., Xia, Z., Liu, B. and Deng, X. "Review of actuators for high speed active flow control", *Science China Technological Sciences*, **55**, pp. 2225-2240 (2012).

14. Zöttl, A. and Stark, H. "Nonlinear dynamics of a microswimmer in Poiseuille flow", *Physical Review Letters*, **108**, p. 218104 (2012).

15. Akiyama, T., Aoki, K.M., Yamamoto, K. and Yoshikawa, T. "Experimental study on vibration-induced convection and heaping in granular beds", *Granular Matter*, **1**, pp. 15-20 (1998).

16. Jang, L.S., Chao, S.H., Holl, M.R. and Meldrum, D.R. "Microfluidic circulatory flows induced by resonant vibration of diaphragms", *Sensors and Actuators A: Physical*, **122**, pp. 141-148 (2005).

17. Gilleron, J., Querbes, W., Zeigerer, A., Borodovsky, A., Marsico, G., Schubert, U., Manygoats, K., Seifert, S., Andree, C. and Stöter, M. "Image-based analysis of lipid nanoparticle-mediated siRNA delivery, intracellular trafficking and endosomal escape", *Nature Biotechnology*, **11**, pp. 638-646 (2013).

18. Keyvani, A. and Strom, K. "A fully-automated image processing technique to improve measurement of suspended particles and flocs by removing out-of-focus objects", *Computers & Geosciences*, **52**, pp. 189-198 (2013).

19. Shah, A.A., Schultz, B., Kohlstedt, K.L., Glotzer, S.C. and Solomon, M.J. "Synthesis, assembly, and image analysis of spheroidal patchy particles", *Langmuir*, **29**, pp. 4688-4696 (2013).

20. Cheong, F.C., Krishnatreya, B.J. and Grier, D.G. "Strategies for three-dimensional particle tracking with holographic video microscopy", *Opt. Express*, **18**, pp. 13563-13573 (2010).

21. Kashdan, J.T., Shrimpton, J.S. and Whybrew, A. "Two-phase flow characterization by automated digital image analysis. Part 2: Application of PDIA for sizing sprays", *Particle & Particle Systems Characterization*, **21**, pp. 15-23 (2004).

22. Wessely, B., Gabsch, S., Altmann, J., Babick, F. "Single particle detection and size analysis with statistical methods from particle imaging data", *Particle & Particle Systems Characterization*, **23**, pp. 165-169 (2006).

23. Wedd, M. "The influence of pixel numbers and image centring upon particle size analysis accuracy", *Particle & Particle Systems Characterization*, **27**(3), pp. 71-75 (2010).

24. Hubner, T., Will, S. and Leipertz, A. "Sedimentation Image Analysis (SIA) for the simultaneous determination of particle mass density and particle size", *Particle & Particle Systems Characterization*, **18**, pp. 70-78 (2001).

25. Kashdan, J.T., Shrimpton, J.S. and Whybrew, A. "Two-phase flow characterization by automated digital image analysis. Part 1: Fundamental principles and calibration of the technique", *Particle & Particle Systems Characterization*, **20**, pp. 387-397 (2003).

26. Dumouchel, C., Grout, S., Leroux, B. and Paubel, X. "Experimental determination of liquid spray drop morphology qualitative information from laser-diffraction measurements", *Particle & Particle Systems Characterization*, **27**(3), pp. 76-88 (2010).

27. Hermawan, M., Bushell, G., Bickert, G. and Amal, R. "Relationship between floc short range structure and sediment compaction", *Particle & Particle Systems Characterization*, **20**, pp. 327-334 (2003).

28. Astrakharchik-Farrimond, E., Shekunov, B.Y., Sawyer, N.B., Morgan, S.P., Somekh, M.G and See, C.W "Particle imaging using a transmission wide-field phase confocal microscope", *Particle & Particle Systems Characterization*, **20**, pp. 104-110 (2003).

29. Serra, C.A. and Chang, Z. "Microfluidic-assisted synthesis of polymer particles", *Chemical Engineering & Technology*, **31**, pp. 1099-1115 (2008).

30. Postnikov, E.B. and I.M. Sokolov "Model of lateral diffusion in ultrathin layered films", *Physica A: Statistical Mechanics and Its Applications*, **391**(21), pp. 5095-5101 (2012).

31. Eral, H.B., Oh, J.M., Van Den Ende, D., Mugele, F. and Duits, M.H. "Anisotropic and hindered diffusion of colloidal particles in a closed cylinder", *Langmuir*, **26**(22), pp. 16722-16729 (2010).

32. Williams, S.J., Park, C. and Wereley, S.T. "Advances and applications on microfluidic velocimetry techniques", *Microfluidics and nanofluidics*, **8**, pp. 709-726 (2010).

33. Peterson, S.D., Chuang, H.S. and Wereley, S.T. "Three-dimensional particle tracking using micro-particle image velocimetry hardware", *Measurement Science and Technology*, **19**, p. 115406 (2008).

34. Guasto, J.S. and Breuer, K.S. "Simultaneous, ensemble-averaged measurement of near-wall temperature and velocity in steady micro-flows using single quantum dot tracking", *Experiments in fluids*, **45**, pp. 157-166 (2008).

35. Sheng, J., Malkiel, E. and Katz, J. "Using digital holographic microscopy for simultaneous measurements of 3D near wall velocity and wall shear stress in a turbulent boundary layer", *Experiments in fluids*, **45**, pp. 1023-1035 (2008).

36. Hao, P.F., Wong, C.Y., Yao, Z.H. and Zhu, K.Q. "Laminar drag reduction in hydrophobic microchannels", *Chemical Engineering & Technology*, **32**, pp. 912-918 (2009).

37. Patrick, M.J., Chen, C.Y., Frakes, D.H., Dur, O. and Pekkan, K. "Cellular -level near-wall unsteadiness of high-hematocrit erythrocyte flow using confocal μPIV", *Experiments in Fluids*, **50**, pp. 887-904 (2011).

Biographies

Mohammad Zabetian Targhi is a PhD degree candidate in the School of Mechanical Engineering at Sharif University of Technology, Tehran, Iran. His research interests include laser-particulate interactions, non-invasive measurement techniques in heat transfer and fluid dynamics, experimental characterization of thermo-fluidic systems, microscopy and image analysis.

Mohammad Behshad Shafii is Associate Professor in the Mechanical Engineering School at Sharif University of Technology, Tehran, Iran. His research interests include fluid diagnostic techniques (MTV, PIV and LIF), heat transfer, phase change, micro-pumps and heat pipes. He is founder and director of the optical diagnostics and heat pipe laboratories.

Mohammad Hassan Saidi is Professor of Mechanical Engineering and Vice President of Academic Affairs at Sharif University of Technology, Tehran, Iran. His current research interests include heat transfer enhancement in boiling and condensation, combustion modeling and simulation, modeling of pulse refrigeration, vortex tube refrigerators, indoor air quality and clean room technology, and energy efficiency in home appliances and desiccant cooling systems.

Mohammad Said Saidi is Professor of Mechanical Engineering at Sharif University of Technology, Tehran, Iran. His research interests include modeling and numerical analysis of transport and deposition of aerosol particles, modeling and numerical analysis of biofluids, modeling and numerical analysis of thermal-hydraulics of porous media and microchannels.

Ramtin Rohani is an MS degree student in the School of Mechanical Engineering at Sharif University of Technology, Tehran, Iran. His research interests include solid-liquid two phase flows, image processing, particle tracking via microscopic imaging, and suspension characterization techniques.